Identification of Induction Motors with Smart Circuit Breakers

L. Fagiano, *Senior Member, IEEE,* M. Lauricella, *Member, IEEE,* D. Angelosante, and E. Ragaini, *Member, IEEE*

***Abstract*—The problem of estimating the parameters of induction motor models is considered, using the data measured by a circuit breaker equipped with industrial sensors. The breaker acquires three-phase stator voltage and current derivative, which are used to formulate an optimization-based identification problem. This setup is novel with respect to the literature, where voltage and current are used. Several algorithmic aspects and improvements are discussed. The presented experimental results indicate that the circuit breaker is able to accurately estimate the machine parameters. The identified motor models can then be used for several applications within a smart grid scenario.**

***Index Terms*—Nonlinear Identification, Parameter Estimation, Induction Motor Identification, Smart Circuit Breakers, Smart Grid, Smart Switchgear**

I. Introduction

In the smart grid paradigm [1], bi-directional flows of electricity and information are exploited to improve and automate grid operation and enable distributed electricity generation. Self-monitoring, self-healing, and advanced load protection and monitoring are crucial smart grid functionalities. However, the realization of these functions requires the installation and connection of a large number of sensing devices, thus increasing complexity and costs.

Circuit breakers represent an ideal candidate to alleviate this problem. Installed in millions across the power grid at all voltage levels, these devices are designed to last tens of years. Circuit breakers can provide a distributed network of sensors and actuators if equipped with sensing, computing and communication capabilities. Since the breakers are already connected to the grid, there is no need to install a separate link to power the sensors and on-board processors. These smart circuit breakers can then accomplish additional functionalities with respect to the classical protection one. An example is the ABB Emax2® breaker, which can also operate as power manager by selectively disconnecting downstream loads to control power consumption [2].

In addition to energy management, another function of interest for smart breakers is the identification of suitable models of the loads, using their electric signature. The identified models can be used e.g. for load detection and monitoring and to discriminate between loads with high inrush currents and faults in the network, as proposed in the patent [3] related to the research presented here. In this paper, we explore this functionality by considering an industrial scenario, where the most common load is represented by electric motors, accounting for about 69% of the whole electricity consumption of the industry sector [4]. In particular, three-phase asynchronous alternating current (AC) induction motors with direct on-line (DOL) connection are most frequently used and they are considered here.

The main problem addressed in this paper is to assess whether the data collected by a commercial circuit breaker can be used to estimate accurately the parameters of an induction motor's model. Our main contribution is to show that indeed this is possible already now. This claim is supported by extensive experimental tests, where we compare the results obtained with a circuit breaker, featuring low-cost industrial sensors, with those obtained with highly accurate and costly laboratory sensors.

The identification of an induction machine's model has been addressed in the literature using e.g. recursive least-squares [5], genetic algorithms [6], extended Kalman filtering [7] or total least-squares plus neurons [8]. In this paper, we resort to a nonlinear optimization approach, as considered e.g. in [9], [10], [11], [12], [13]. All these works assume the availability of stator voltage, current and often also rotor speed measurements, and they do not treat in detail aspects like sensitivity of the estimation procedure to initialization, stability of the estimated parameters with respect to the sampling frequency, and efficiency of the employed optimization routine. However, these are crucial issues from the point of view of control system technology implementation. As additional original contributions, in this paper we use stator voltage and current derivatives (i.e. the measurements provided by the circuit breaker) and we present several results concerning implementation aspects, from explicit gradient computation in the optimization routine to different numerical integration techniques. These contributions are also novel with respect to our recent work [14], in which we considered only forward Euler integration and we made no attempt to improve the efficiency of the identification routine. The paper is organized as follows. Section II introduces the experimental setup that we built to carry out our tests and the formulation of the parameter identification problem. Section III presents the chosen induction machine model and describes the available measurements. Section IV describes the considered nonlinear identification approach and the implementation aspects. Experimental results are discussed in Section V, and conclusions and future developments in Section VI.

L. Fagiano and M. Lauricella are with the Dipartimento di Elettronica, Informazione e Bioingegneria, Politecnico di Milano. D. Angelosante is with ABB Switzerland, Corporate Research. E. Ragaini is with ABB Italia SpA. E-mail addresses: {lorenzo.fagiano | marco.lauricella}@polimi.it; daniele.angelosante@ch.abb.com; enrico.ragaini@it.abb.com.

Corresponding author: Lorenzo Fagiano.

II. System description and problem formulation

The layout of the considered experimental setup is shown in Fig. 1. A picture of the setup, realized at ABB Corporate Research Center in Poland, is shown in Fig. 2. The network voltage is 380 VAC phase-to-phase, 50 Hz. Referring to Fig. 1, the system includes the following elements:

- An ABB Emax2® circuit breaker with 800 A (rms) of nominal current, which measures the three phase voltage (phase-to-phase measurements) via a resistive divider, and the three-phase current derivatives via Rogowski coils;
- Two induction motors, $M1$ and $M2$, and two contactors (ABB AF38 series) to connect each motor to the 3-phase line. Motor $M1$ is Y-connected, while $M2$ is Δ-connected.
- Two sensor boxes, built at ABB Corporate Research Center Switzerland, equipped with high-cost three-phase voltage and current sensors based on Hall-effect transducers, and with a relay to send open/close control signals to the contactors;
- A Real-Time machine, which logs the data acquired by the circuit breakers and the sensor boxes, and sends the open/close commands to the contactors via the sensor boxes. The Real-Time machine is operated by the testing personnel via a Human-Machine Interface, to carry out the desired testing sequences.

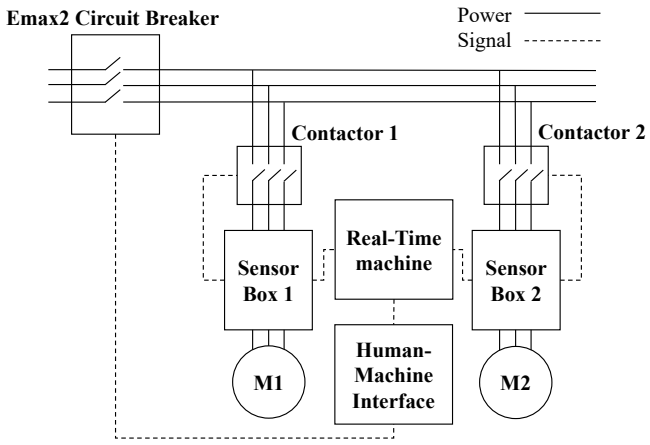

Fig. 1. Layout of the employed experimental setup.

The main features of the employed motors, sensors, and data acquisition systems are provided in [15]. The sensor boxes feature highly accurate transducers: the corresponding measured data is used as "ground truth" to evaluate the performance achieved with the data collected by the circuit breaker, which is the object of study. The experimental tests considered in this work are direct-on-line motor startups, in which both contactors are initially open. Then, upon command by the test personnel, the Real-Time machine sends a triggering signal to one of the two contactors and acquires the electric signature of the corresponding motor, as measured both by its sensor box and by the smart breaker. This testing procedure is well-motivated by the possibility, in a real-world application, to carry out several motor startups in the commissioning phase

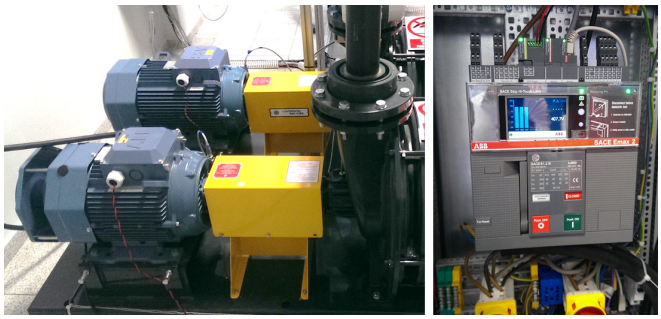

Fig. 2. Pictures of the experimental setup. Left: induction motors employed for the tests. Right: Emax2® breaker installed in the electric cabinet of the testing laboratory.

of a new installation, in order to record the electric signature of each machine in a controlled way for the sake of parameter estimation.

Given the batch of data obtained in the start-up tests, our goal is to identify the parameters of a model of each motor, where the inputs are the stator voltages, and the measured outputs are either the stator currents (for sensor box data) or their derivatives (for circuit breaker data). In particular, we seek the parameter values that minimize a simulation-error performance criterion. The cost function is in fact based on the error between the measured outputs and those computed by simulating the model from known initial condition (standstill), applying in open loop the measured input (i.e. voltage) values. We note that this identification procedure is not meant to be performed in real-time, differently from observers such as the extended Kalman filter. Rather, the parameter estimation can be carried out either by the breaker itself in a low-priority task in parallel to the standard (high priority) safety functionalities (e.g. fault detection and intervention curve evaluation), or by external computation, e.g. through a cloud service. Smart circuit breakers like the considered one are in fact equipped with Internet connection. Therefore, there is no strict computational time limit for the approach presented in this paper. A sensible application is condition monitoring of the motor and/or its load: by repeating the identification procedure at each motor startup, for example, one could identify possible changes over time of the estimated parameters, which could then be linked to possible wear of components or changes in the load connected to the motor.

III. Induction machine model and experimental data-set

We resort to a rather standard dynamical model of three-phase induction motors (see e.g. [16]), summarized here for the sake of completeness. In the remainder, t denotes the continuous time variable, a, b, c the motor phases, s and r stator and rotor quantities, respectively. We indicate with $\boldsymbol{v}_{abc,s}(t) := [v_{as}(t)\ v_{bs}(t)\ v_{cs}(t)]^T$ the stator voltages, with $\boldsymbol{i}_{abc,s}(t) := [i_{as}(t)\ i_{bs}(t)\ i_{cs}(t)]^T$ the stator currents, and with $\boldsymbol{v}_{abc,r}(t) := [v_{ar}(t)\ v_{br}(t)\ v_{cr}(t)]^T$ and $\boldsymbol{i}_{abc,r}(t) := [i_{ar}(t)\ i_{br}(t)\ i_{cr}(t)]^T$ the rotor voltages and currents, respectively. As usual, we transform three-phase quantities into two-phase ones through a change of variables, which implies the

choice of a common reference frame (see [16]). Here, we adopt the stator (i.e. fixed) reference frame. This choice has the advantage that we can directly compare the model outputs with the measured stator voltage and current (or current derivative) provided by the employed sensors. Since the electric machines at hand are balanced, the use of a static frame results in the following transformation matrix:

$$\boldsymbol{M} := \frac{2}{3}\begin{bmatrix} 1 & \cos\left(-\frac{2}{3}\pi\right) & \cos\left(\frac{2}{3}\pi\right) \\ 0 & \sin\left(-\frac{2}{3}\pi\right) & \sin\left(\frac{2}{3}\pi\right) \\ 0.5 & 0.5 & 0.5 \end{bmatrix}.$$

The matrix $\boldsymbol{M}$, when multiplied by a three-phase quantity $\boldsymbol{s}_{abc} := [s_a \ s_b \ s_c]^T$ results in a vector $\boldsymbol{s}_{dq0} = [s_d \ s_q \ 0]^T$, i.e. with only two independent components, commonly referred to as the *dq*-components. In the following, we denote with $\boldsymbol{s}_{dq}$ the 2-dimensional vectors in *dq*-components, where we dropped the zero component for simplicity.

The electrical torque $T_e(t)$ and the load torque $T_l(t)$ are modeled as:

$$T_e(t) = \frac{3N_p}{4\omega_e}\left(\psi_{qr}(t)i_{dr}(t) - \psi_{dr}(t)i_{qr}(t)\right) \tag{1}$$

$$T_l(t) = T_{l_0} + T_{l_1}\,\omega_r(t) \tag{2}$$

where ω_e is the nominal grid frequency in rad/s, $\psi(t)$ is the flux per time unit, $\omega_r(t)$ is the rotor angular speed, N_p is the number of poles of the motor, J_r is the rotor moment of inertia, and T_{l_0} and T_{l_1} are, respectively, a constant load coefficient and a constant viscous friction coefficient. This load model is over-parametrized with respect to our experimental setup, where the constant term is zero and a only a linear viscous term is present (we discuss the effects of over-parametrization in the experimental results of Section V). With a straightforward extension, one can also consider a second-order equation to model the load, i.e. $T_l(t) = T_{l_0} + T_{l_1}\omega_r(t) + T_{l_2}\omega_r(t)^2$. This is typical for loads that manipulate a fluid or gas, such as fans and pumps. The model input is the stator voltage in its *dq*-representation, $\boldsymbol{u}(t) := [v_{ds}(t) \ v_{qs}(t)]^T \in \mathbb{R}^2$, and its state is the vector $\boldsymbol{x}(t) := [\psi_{ds}(t) \ \psi_{qs}(t) \ \psi_{dr}(t) \ \psi_{qr}(t) \ \omega_r(t)]^T \in \mathbb{R}^5$. We are now in position to write the model equations (where $\dot{x} \doteq dx/dt$ denotes the time derivative):

$$\dot{\boldsymbol{x}}(t) = \boldsymbol{A}(\omega_r(t))\boldsymbol{x}(t) + \boldsymbol{B}\boldsymbol{u}(t) + \boldsymbol{\beta}(\boldsymbol{x}(t)) \tag{3}$$

where

$$\boldsymbol{A}(\omega_r(t)) = \omega_e \begin{bmatrix} \frac{R_s(X_m-X_l)}{X_l^2} & 0 & \frac{R_s X_m}{X_l X_l} & 0 & 0 \\ 0 & \frac{R_s(X_m-X_l)}{X_l^2} & 0 & \frac{R_s X_m}{X_l X_l} & 0 \\ \frac{R_r X_m}{X_l X_l} & 0 & \frac{R_r(X_m-X_l)}{X_l^2} & -\frac{\omega_r(t)}{\omega_e} & 0 \\ 0 & \frac{R_r X_m}{X_l X_l} & \frac{\omega_r(t)}{\omega_e} & \frac{R_r(X_m-X_l)}{X_l^2} & 0 \\ 0 & 0 & 0 & 0 & 0 \end{bmatrix};$$

$$\boldsymbol{B} = \begin{bmatrix} \omega_e & 0 \\ 0 & \omega_e \\ 0 & 0 \\ 0 & 0 \\ 0 & 0 \end{bmatrix}; \quad \boldsymbol{\beta}(\boldsymbol{x}(t)) = \begin{bmatrix} 0 \\ 0 \\ 0 \\ 0 \\ \frac{N_p}{2J_r}\left(T_e(t) - T_l(t)\right) \end{bmatrix}. \tag{4}$$

In (4), R_s is the stator resistance, R_r is the rotor resistance, X_l and X_m are respectively the stator (and rotor) reactance and the magnetizing reactance at the nominal electric frequency. The output equations depend on the measured quantity, which can be either the stator current or its derivative (depending on the considered measuring equipment, see Section II). The output variables are again transformed in *dq*-components. We indicate with $\boldsymbol{y}_{SB}(t)$ the output vector obtained with current measurements (i.e. from the sensor boxes, see Section II) and with $\boldsymbol{y}_{CB}(t)$ the one given by current derivative measurements (i.e. from the circuit breaker). Thus, in the first case we have:

$$\boldsymbol{y}_{SB}(t) = \underbrace{\frac{1}{X_l}\begin{bmatrix} 1-\frac{X_m}{X_l} & 0 & -\frac{X_m}{X_l} & 0 & 0 \\ 0 & 1-\frac{X_m}{X_l} & 0 & -\frac{X_m}{X_l} & 0 \end{bmatrix}}_{\boldsymbol{C}} \boldsymbol{x}(t). \tag{5}$$

If current derivative measurements are considered, we have:

$$\boldsymbol{y}_{CB}(t) = \boldsymbol{C}\dot{\boldsymbol{x}}(t). \tag{6}$$

Equations (1)-(6) provide the continuous time model of the motor considered in this paper. The vector of parameters to be identified from experimental data is denoted by $\boldsymbol{p} = [R_s \ R_r \ X_l \ X_m \ J_r \ T_{l_0} \ T_{l_1}]^T$, $\boldsymbol{p} \in \mathbb{R}^7$, while the number of poles N_p is assumed known, since it is easily obtained from the motor nameplate or data-sheet.

The model parameters will be estimated using the collected data sets, which are described next. We indicate with t_s the sampling period (and with $f_s = 1/t_s$ the sampling frequency), with N the total number of samples, and with $\tilde{\cdot}$ the measured (i.e. affected by noise) quantities. As regards the sensor boxes, the voltage data matrix $\tilde{\boldsymbol{V}}_{SB}$ is given by:

$$\tilde{\boldsymbol{V}}_{SB} = \begin{bmatrix} \tilde{v}_{ds,SB}(t_s), \cdots, \tilde{v}_{ds,SB}(N\,t_s) \\ \tilde{v}_{qs,SB}(t_s), \cdots, \tilde{v}_{qs,SB}(N\,t_s) \end{bmatrix},$$

where $\tilde{v}_{ds,SB}(t)$, $\tilde{v}_{qs,SB}(t)$ are the *dq*-components of the stator voltages acquired by the voltage transducers in the sensor boxes. Similarly, the current data matrix $\tilde{\boldsymbol{I}}$ is:

$$\tilde{\boldsymbol{I}} = \begin{bmatrix} \tilde{i}_{ds}(t_s), \cdots, \tilde{i}_{ds}(Nt_s) \\ \tilde{i}_{qs}(t_s), \cdots, \tilde{i}_{qs}(Nt_s) \end{bmatrix}.$$

For the smart circuit breaker we have the voltage data matrix $\tilde{\boldsymbol{V}}_{CB}$, defined like $\tilde{\boldsymbol{V}}_{SB}$ but containing the measures $\tilde{v}_{ds,CB}(t)$, $\tilde{v}_{qs,CB}(t)$ acquired by the transducers in the breaker, and the current derivative data matrix $\dot{\tilde{\boldsymbol{I}}}$:

$$\dot{\tilde{\boldsymbol{I}}} = \begin{bmatrix} \dot{\tilde{i}}_{ds}(t_s), \cdots, \dot{\tilde{i}}_{ds}(Nt_s) \\ \dot{\tilde{i}}_{qs}(t_s), \cdots, \dot{\tilde{i}}_{qs}(Nt_s) \end{bmatrix}.$$

IV. Identification procedure

The parameter identification problem is cast into an off-line nonlinear least squares estimation, where a batch of data collected during the motor start-up transient is compared with the corresponding simulated quantities, obtained by integrating the model from known initial condition and applying the acquired stator voltage data. The resulting numerical optimization problem takes the general form:

$$\hat{\boldsymbol{p}} = \arg\min_{\boldsymbol{p}\in\mathcal{P}} tr(\boldsymbol{J}(\boldsymbol{p})) \tag{7a}$$

subject to

discrete-time model equations (7b)

where $tr(\cdot)$ indicates the trace of a matrix, $\boldsymbol{J}(\boldsymbol{p})$ is a square cost matrix, and $\mathcal{P}$ is a set of admissible parameters, defined e.g. by box constraints that account for sensible upper and lower bounds on each component of $\boldsymbol{p}$, e.g. positivity constraints on resistance and reactance values. The constraints (7b) account for the model equations described in Section III, suitably discretized in order to numerically integrate them.

In this paper, we consider and compare different alternatives for the discrete-time model equations in (7b) and for the cost matrix $\boldsymbol{J}(\boldsymbol{p})$ in (7a), as detailed in the following sub-sections.

A. Model discretization

The induction motor model has to be discretized for the sake of numerical integration. Since the measurements coming from the sensor boxes and the smart circuit breaker are acquired with sampling period t_s, we decided to integrate the model numerically with a fixed integration step equal to t_s. Albeit not strictly necessary (since one can in principle employ a smaller integration step and then consider, to compute the fitting errors, the model outputs at the time instants when the experimental data have been sampled), this choice simplifies the identification procedure and its implementation on industrial hardware. We tested the performance and properties of the estimation algorithm at different sampling rates (and corresponding integration steps), using either a well-established numerical integration technique, the forward Euler method, or a discretization approach that we called "Input Preview" method.

Discretizing the state equation (3) with the forward Euler method yields:

$$\hat{\boldsymbol{x}}(k+1) = \Big(\boldsymbol{I} + t_s \boldsymbol{A}(\hat{\omega}_r(k))\Big)\hat{\boldsymbol{x}}(k) + t_s \boldsymbol{B}\boldsymbol{u}(k) + t_s \boldsymbol{\beta}(\hat{\boldsymbol{x}}(k)), \tag{8}$$

where $\boldsymbol{I}$ is the identity matrix.

On the other hand, the discrete-time expression of (3) obtained using the Input Preview method is:

$$\begin{aligned} &\hat{\boldsymbol{x}}(k+1) = \\ &\left(\boldsymbol{I} - \frac{t_s}{2}\boldsymbol{A}(\hat{\omega}_r(k))\right)^{-1} \left(\left(\boldsymbol{I} + \frac{t_s}{2}\boldsymbol{A}(\hat{\omega}_r(k))\right)\hat{\boldsymbol{x}}(k) + \right. \\ &\left. + \frac{t_s}{2}\boldsymbol{B}\Big(\boldsymbol{u}(k+1) + \boldsymbol{u}(k)\Big) + t_s \boldsymbol{\beta}(\hat{\boldsymbol{x}}(k))\right) \end{aligned} \tag{9}$$

with $\hat{\boldsymbol{x}}(0) = 0$. This discretization approach is inspired in a sense by the Tustin method, whose original formulation cannot be used here due to the model nonlinearity. Still, in the Input Preview we consider the one-step-ahead input value $u(k+1)$, and the "forward projection" of the linear part of the system's dynamics, given by $\left(I - \frac{t_s}{2}\boldsymbol{A}(\omega_r(k))\right)^{-1}$. In the latter matrix inversion, in principle $\boldsymbol{A}(\omega_r(k+1))$ should be used (compare (4)). However, to retain a computationally efficient solution, we adopted the approximation $\hat{\omega}_r(k+1) \simeq \hat{\omega}_r(k)$, which is reasonable since the rotor speed dynamics are significantly slower than the electrical time constants of the machine. As the experimental results presented in Section V show, the Input Preview method achieves better performance than the forward Euler one, while still retaining a reasonably low computational complexity (since it does not require an iterative numerical solution at each time step, like implicit integration methods do). Moreover, as discussed in Section IV-C, both methods allow us to derive an explicit calculation of parametric sensitivities, which we exploit to compute the cost function's gradient and estimate its Hessian. The latter aspect greatly improves the computational efficiency when solving the identification problem.

Finally, the model initial condition is $\hat{\boldsymbol{x}}(0) = 0$, and the input vector $\boldsymbol{u}(k)$ corresponds to the $k-$th column of either matrix $\tilde{\boldsymbol{V}}_{SB}$ (for sensor box data) or $\tilde{\boldsymbol{V}}_{CB}$ (for circuit breaker data). Regarding the output equations, these are equal to the continuous-time ones, since they are static relationships. Thus, for stator currents we have:

$$\hat{\boldsymbol{y}}_{SB}(k) = \boldsymbol{C}\hat{\boldsymbol{x}}(k), \tag{10}$$

while for stator current derivatives we have:

$$\hat{\boldsymbol{y}}_{CB}(k) = \boldsymbol{C}\dot{\hat{\boldsymbol{x}}}(k), \tag{11}$$

where $\dot{\hat{\boldsymbol{x}}}(k) = \boldsymbol{A}(\hat{\omega}_r(k))\hat{\boldsymbol{x}}(k) + \boldsymbol{B}\boldsymbol{u}(k) + \boldsymbol{\beta}(\hat{\boldsymbol{x}}(k))$. Each one of the output equations (10) and (11) can be combined with either (8) or (9) and inserted in the constraints (7b) to obtain four possible cases, i.e. Euler or Input Preview discretization and either current or current derivative as measured output. In the literature, to the best of our knowledge, only the case of Euler integration and current as output has been considered so far, while here we explore all four combinations.

B. Cost function definition

The matrix $\boldsymbol{J}(\boldsymbol{p})$ in (7a) is different depending on whether current or current derivative data are employed in the fitting criterion. In case of stator current data (i.e. acquired by the sensor boxes in our setup), the cost is computed as

$$\boldsymbol{J}_{SB}(\boldsymbol{p}) = \left(\Big(\tilde{\boldsymbol{I}} - \hat{\boldsymbol{Y}}(\tilde{\boldsymbol{V}}_{SB}, \boldsymbol{p})\Big)\Big(\tilde{\boldsymbol{I}} - \hat{\boldsymbol{Y}}(\tilde{\boldsymbol{V}}_{SB}, \boldsymbol{p})\Big)^T\right) \tag{12}$$

where $\hat{\boldsymbol{Y}}(\tilde{\boldsymbol{V}}_{SB}, \boldsymbol{p}) := [\hat{\boldsymbol{y}}_{SB}(1), \cdots, \hat{\boldsymbol{y}}_{SB}(N)] \in \mathbb{R}^{2\times N}$ is a matrix containing the stator current signals in the *dq*-components simulated with the motor model (either (8) or (9)) and the output equation (10), excited by the stator voltage signal $\tilde{\boldsymbol{V}}_{SB}$ as input. In the case of stator current derivative data (i.e. acquired by the breaker), the cost is computed as

$$\boldsymbol{J}_{CB}(\boldsymbol{p}) = \left(\Big(\tilde{\dot{\boldsymbol{I}}} - \hat{\dot{\boldsymbol{Y}}}(\tilde{\boldsymbol{V}}_{CB}, \boldsymbol{p})\Big)\Big(\tilde{\dot{\boldsymbol{I}}} - \hat{\dot{\boldsymbol{Y}}}(\tilde{\boldsymbol{V}}_{CB}, \boldsymbol{p})\Big)^T\right) \tag{13}$$

where $\hat{\dot{\boldsymbol{Y}}}(\tilde{\boldsymbol{V}}_{CB}, \boldsymbol{p}) := [\hat{\boldsymbol{y}}_{CB}(1), \cdots, \hat{\boldsymbol{y}}_{CB}(N)]$ contains the simulated stator current derivative signals in the *dq*-components, obtained by integrating the motor model with the output equation (11) and applying the measured voltage sequence $\tilde{\boldsymbol{V}}_{CB}$ as input.

C. Algorithmic aspects: explicit gradient computation and Hessian estimates, parameter initialization

We solve the optimization problem (7) with a constrained Gauss-Newton algorithm [17], where we compute the gradient

of the cost function and estimate its Hessian by exploiting the problem structure. In particular, $J(\boldsymbol{p})$ can be re-written as

$$\boldsymbol{J}(\boldsymbol{p}) = \boldsymbol{F}(\boldsymbol{p})^T \boldsymbol{F}(\boldsymbol{p}), \tag{14}$$

where $\boldsymbol{F}(\boldsymbol{p}) \in \mathbb{R}^{2N}$ is a vector containing the differences between the measured outputs (currents or their derivatives) and the model outputs at each time step. To compute the Jacobian matrix $\nabla_{\boldsymbol{F}}(\boldsymbol{p})$ of $\boldsymbol{F}(\boldsymbol{p})$, we differentiate the model equations with respect to the model parameters, resulting in a recursive formulation that can be computed together with the model integration. Such a recursion is described in [15] for both Euler and Input Preview methods. Then, the gradient of $\boldsymbol{J}(\boldsymbol{p})$ is computed as:

$$\nabla_{\boldsymbol{J}}(\boldsymbol{p}) = 2\nabla_{\boldsymbol{F}}(\boldsymbol{p})^T \boldsymbol{F}(\boldsymbol{p}),$$

and, by considering the Taylor expansion of $\boldsymbol{F}(\boldsymbol{p})$ truncated at the first order and inserted in (14), the Hessian of $\boldsymbol{J}(\boldsymbol{p})$ is approximated as

$$\nabla^2_{\boldsymbol{J}}(\boldsymbol{p}) \simeq \nabla_{\boldsymbol{F}}(\boldsymbol{p})^T \nabla_{\boldsymbol{F}}(\boldsymbol{p}).$$

In our experiments, the use of this approach resulted in significant computational savings with respect to general-purpose nonlinear programming solvers, as we mention in Section V.

Another relevant aspect from the point of view of computational efficiency is the initialization of the optimization routine. Due to the non-convex nature of the problem, the algorithm generally converges to a local optimum. The sub-optimality of the solution and the convergence speed clearly depend on the initialization of the parameters in the SQP solver. One possible approach to attain the global optimum is to run several times the algorithm with different initialization values, generated randomly within the set $\mathcal{P}$, and then to consider the estimate providing the smallest cost function value. In Section V, we analyze how the sensitivity to initialization changes with different sampling frequencies and discretization methods. A related problem is the possibility that, during the numerical optimization, the solver sets parameter values that render the state and output trajectories unstable. However, these parameter values are naturally rejected, since they inevitably produce large errors with respect to the measured data-set used in the cost function. Since the time horizon of the data is finite and rather short, numerical divergence problems are not an issue.

V. Experimental results

Using the experimental rig described in Section II, we collected about 100 direct on-line start-up transients of the 3-phase induction motors. We considered different sampling frequencies and, for each motor, we employed the data from one start-up experiment for the identification, and the data of three additional experiments for validation. As performance metric, to compare the different tests, we consider the Normalized Mean Prediction Error. This is computed as $\text{NMPE} := \sqrt{tr\left(\left(\tilde{\boldsymbol{I}} - \hat{\boldsymbol{Y}}(\tilde{\boldsymbol{V}}_{SB}, \hat{\boldsymbol{p}})\right)\left(\tilde{\boldsymbol{I}} - \hat{\boldsymbol{Y}}(\tilde{\boldsymbol{V}}_{SB}, \hat{\boldsymbol{p}})\right)^T\right) / tr\left(\tilde{\boldsymbol{I}}\tilde{\boldsymbol{I}}^T\right)}$. Note that in the NMPE calculation we always compare the model predictions with the motor current and voltage measured by the high-quality sensors installed in the sensor boxes. This means that also the parameters estimated from the smart breaker data (i.e. using current derivatives as identification data-set) are then tested by comparing the resulting simulated currents with the high-quality measures collected by the sensor boxes. In all the results presented in the following, we provide the range of NMPE values obtained in the three validation experiments related to each specific test case. As regards the set of admissible parameters $\mathcal{P}$, we selected rather wide ranges for each of the variables to be estimated, given by non-negative values of $\boldsymbol{p}$ such that $\boldsymbol{p} \preceq \begin{bmatrix}100 & 100 & 100 & 500 & 20 & 100 & 0.35\end{bmatrix}^T$. In all the tests reported in the following, we employed the SQP solver based on the constrained Gauss-Newton approach and analytic computation of the gradient, as described in Section IV-C. The solver, implemented in MatLab, was able to converge on average in about 20 iterations and 120 s on a Laptop equipped with Intel i7 dual-core processor with 2.4 GHz clock speed and 8 GB of RAM. For a comparison, on the same hardware a standard optimization routine (MatLab `fmincon`) took on average 50 iterations and 2200 s with the same termination tolerances.

Sensors comparison. To determine whether the data collected by the industrial voltage and current sensors installed in the considered commercial circuit breaker are good enough to identify the model parameters, we compared the results of the estimation procedure performed using data acquired by the sensor boxes, which have as maximum sampling frequency 5 kHz, with the results obtained using data measured by the smart breaker, where we selected a sampling frequency of 4.8 kHz from the available values (see [15] for the sensors' specifications). In both cases, the discrete-time model is obtained using the Input Preview method. The results related to motor $M1$ are presented in Table I. It can be noted that the differences between the two parameter estimates and the resulting NMPE ranges are not significant.

TABLE I
MOTOR $M1$ - IDENTIFIED PARAMETERS: COMPARISON BETWEEN THE RESULTS OBTAINED WITH SENSOR BOX DATA AND CIRCUIT BREAKER DATA.

	Sensor box	Circuit breaker
R_s	0.48	0.48
R_r	0.20	0.21
X_l	0.29	0.30
X_m	11.92	11.29
J_r	0.26	0.26
T_{l_0}	0	0
T_{l_1}	0.039	0.037
NMPE %	8.115 ± 0.015	7.865 ± 0.115

Figs. 3(a) and 3(b) show the comparison between the q component of the stator current, measured by the sensor box during a validation experiment, and the signal reconstructed using the parameters identified from the sensor box data-set and from the circuit breaker data-set. The fitting is good in both cases, as expected from the NMPE results of Table I. Figs. 3(c) and 3(d) present the comparison between the q component of the stator current derivatives, measured by the smart circuit

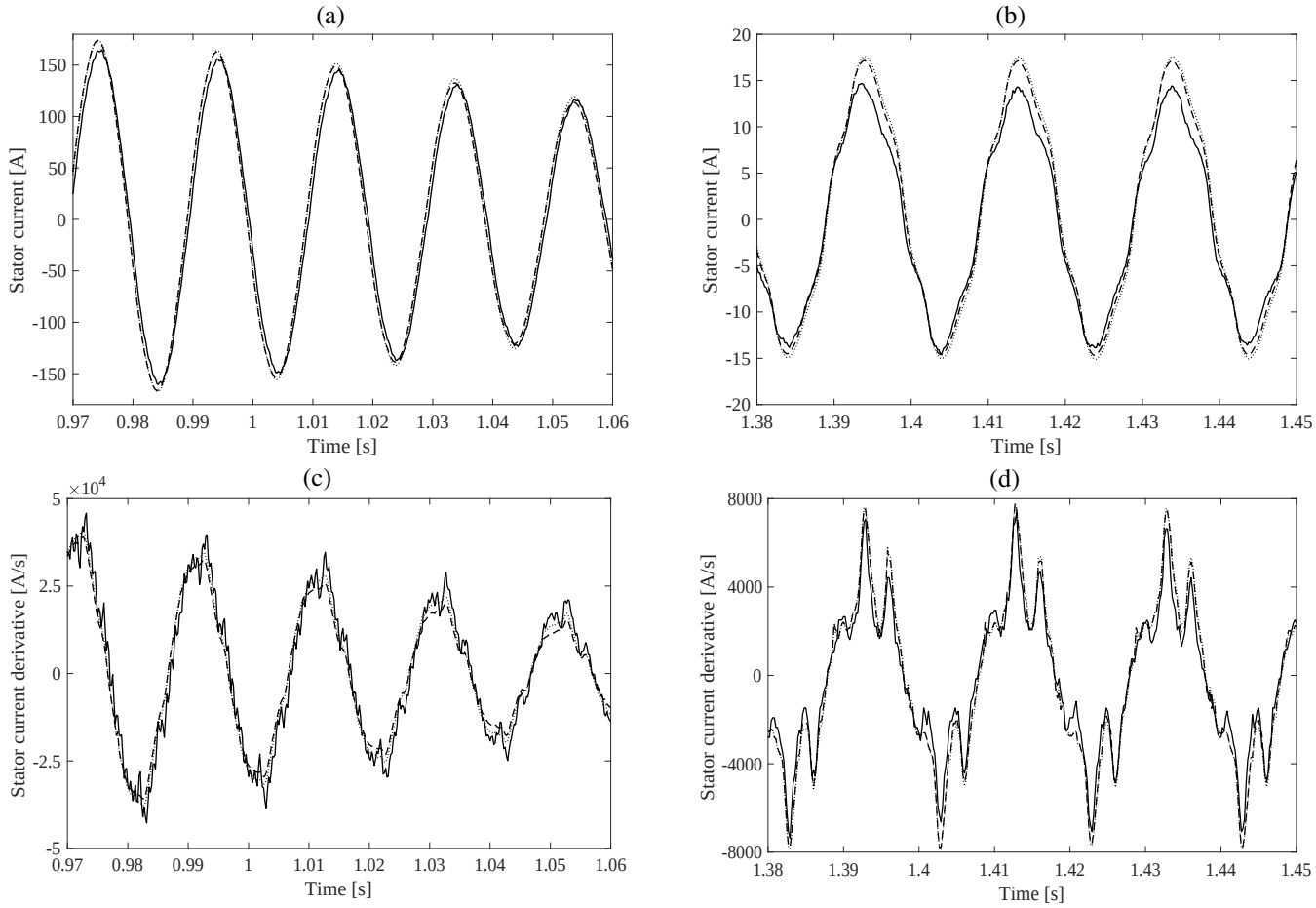

Fig. 3. Motor $M1$ - Validation of the estimated parameters. Comparison between simulated and measured current signals acquired by sensor box (plots (a) and (b)), and between simulated and measured current derivative signals acquired by the smart circuit breaker (plots (c) and (d)). The plots on the left pertain to the first part of the transient, while those on the right pertain to a steady speed condition. Solid lines: measured q component of stator current (or current derivative); dashed lines: simulated q component based on parameters estimated from sensor box data: dotted lines: simulated q component based on parameters estimated from circuit breaker data.

breaker during the validation experiment, and the current derivatives reconstructed using the parameters identified from the two different data-sets described before. Also in this case the fitting is good and the parameters estimated from the two different data-sets have a comparable performance.

Table II presents the comparison between the parameters of motor $M2$ estimated from sensor box data and from smart circuit breaker data. The obtained results are fully aligned with those of motor $M1$.

These results indicate that it is possible to obtain a good estimate of the motor parameters also using data acquired by Rogowski coil sensors of commercial circuit breakers, where the stator current derivatives are measured in place of a direct measure of the stator currents. In the remainder of this section, we investigate more in detail the performance of the estimation algorithm using the data acquired by the smart circuit breaker, with different choices of discretization method and sampling frequency, and we analyze the sensitivity to parameter initialization and model over-parametrization.

Comparison between discretization methods. We applied the estimation algorithms derived using the two discretization methods described in Section IV-A to data-sets acquired by the circuit breaker with various sampling frequencies. Table III contains the parameter values identified using one data-set acquired at $f_s = 4.8$ kHz, and another one at $f_s = 2.4$ kHz. In the table, we highlight in bold the parameter values that are clearly different from the best ones, reported previously in Table I. For the case of data acquired with $f_s = 4.8$ kHz, the results of the estimation procedure based on the two discretization methods are similar. On the other hand, the data-set acquired with $f_s = 2.4$ kHz leads to significantly different

TABLE II
MOTOR $M2$ - IDENTIFIED PARAMETERS: COMPARISON BETWEEN THE RESULTS OBTAINED WITH SENSOR BOX DATA AND CIRCUIT BREAKER DATA.

	Sensor box	Circuit breaker
R_s	1.15	1.12
R_r	0.49	0.49
X_l	0.70	0.71
X_m	33.67	34.48
J_r	0.27	0.28
T_{l_0}	0	0
T_{l_1}	0.035	0.031
NMPE %	8.675 ± 0.145	9.65 ± 0.11

results: the estimates obtained with the forward Euler method are not consistent with those obtained by the same method at higher frequency, and the NMPE values are much larger. The estimates obtained with the Input Preview method appear to be resilient to lower frequencies, and they are still very close to the best ones. We analyzed more in detail the sensitivity of

TABLE III
MOTOR $M1$ - IDENTIFIED PARAMETERS: COMPARISON BETWEEN DIFFERENT DISCRETIZATION METHODS. WE HIGHLIGHT IN BOLD THE PARAMETERS THAT ARE SIGNIFICANTLY DIFFERENT FROM THE OPTIMUM ONES.

	Input Preview	
	4.8 kHz	2.4 kHz
R_s	0.48	0.48
R_r	0.21	0.21
X_l	0.30	0.30
X_m	11.29	11.28
J_r	0.26	0.26
T_{l_0}	0	0
T_{l_1}	0.037	0.037
NMPE %	7.865 ± 0.115	7.875 ± 0.035

	Forward Euler	
	4.8 kHz	2.4 kHz
R_s	0.53	0.55
R_r	0.22	0.24
X_l	0.28	0.26
X_m	**2.52**	**1.45**
J_r	0.24	0.19
T_{l_0}	0	**13.21**
T_{l_1}	**0.13**	**0.20**
NMPE %	11.55 ± 0.07	$\mathbf{33.025 \pm 0.345}$

the estimation results to the sampling frequency by running the algorithm on data with f_s spacing from 1.2 kHz to 9.6 kHz. An example of the obtained results is depicted in Fig. 4: it is evident that, in the case of forward Euler method, the identified parameters change sensibly with the sampling frequency, while, in the Input Preview case, they exhibit a much lower variability. The reported results further confirm that the Input Preview method is generally more stable with respect to variations of the sampling frequency of the measured data (and size of the integration step), while the forward Euler estimate diverges at low frequencies.

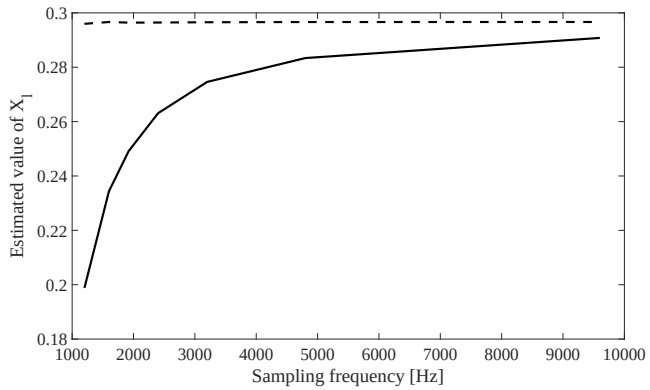

Fig. 4. Motor $M1$ - circuit breaker data, sensitivity to data sampling frequency. Estimated value of the reactance X_l as a function of the data sampling frequency: estimation algorithm based on the forward Euler method (solid line) and on the Input Preview method (dashed).

Sensitivity to parameter initialization. To analyze the sensitivity of the algorithm to initialization, we performed 1000 estimation routines on the same data-set, where we randomly picked the initial parameter vector $\boldsymbol{p}_0$ with a uniform distribution over a sub-set of $\mathcal{P}$, given by all the non-negative values of $\boldsymbol{p}_0$ such that $\boldsymbol{p}_0 \preceq \begin{bmatrix}10 & 10 & 10 & 15 & 2 & 1 & 0.042\end{bmatrix}^T$. Note that the value of $\boldsymbol{p}$ that we consider as the global optimum is inside the described set (compare Table I). We repeated this analysis considering either 2.4 kHz or 4.8 kHz and, for each frequency, either forward Euler or Input Preview method. We considered as acceptable the result when the obtained value of the cost $\boldsymbol{J}(\hat{\boldsymbol{p}})$ was inside the interval $[\boldsymbol{J}_{min},\ 1.05 \cdot \boldsymbol{J}_{min}]$, where $\boldsymbol{J}_{min}$ is the minimum cost value across all 1000 tests for the specific combination of sampling frequency and discretization method. The results are reported in Table IV.

TABLE IV
MOTOR $M1$ - NUMBER OF ACCEPTABLE ESTIMATION RESULTS FOR UNIFORMLY DISTRIBUTED RANDOM-GENERATED INITIAL PARAMETERS.

	Input Preview	Euler
$f_s = 4.8$ kHz	756 over 1000	703 over 1000
$f_s = 2.4$ kHz	159 over 1000	7 over 1000

It is clear that the sensitivity increases as the sampling frequency decreases, and that the Input Preview method is generally more resilient to initialization. Fig. 5 illustrates the distribution of the minimum cost obtained by the estimation routines in the 1000 trials, normalized by the corresponding value of $\boldsymbol{J}_{min}$ considered as the optimum. These figures show how often the algorithm reaches the best fitting cost and how the results are distributed around local minima with different degrees of sub-optimality. When the estimation algorithm falls in a sub-optimal local minimum, the corresponding estimated parameters can be significantly different from the globally optimum ones, reaching in some cases values that are 3 to 50 times larger than the best ones.

Effects of over-parametrization. In this work we adopted

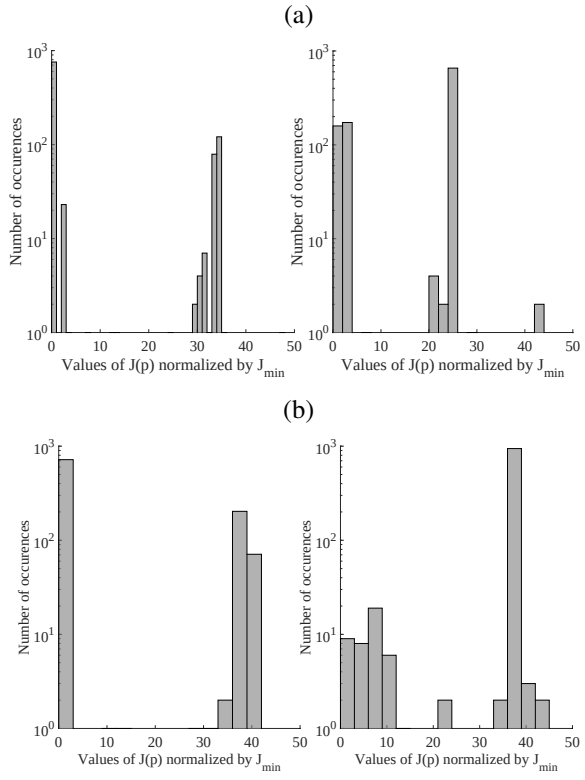

Fig. 5. Motor $M1$ - Convergence analysis of 1000 estimation routines with randomly generated initial parameters. Identification data measured by the circuit breaker. Discretization method: (a) Input Preview, (b) Forward Euler. Sampling frequency: 4.8 kHz (left plots) and 2.4 kHz (right plots).

a load torque model based on two parameters, i.e. a constant term and a linear one in the rotor speed. In the experimental setup, as described in Section II, we know a priori that only the linear term is different from zero. We thus analyzed how the estimation results vary if we use a load model with only the linear term, which corresponds to the actual behavior of our experimental setup. In Table V we compare the results of the estimation algorithm applied to data acquired with different sampling frequencies, in the case of the over-parametrized load torque model and in the case of linear viscous term only. From these results, it is clear that the Input Preview method is sufficiently robust to provide good performance also in case of over-parametrized load model; on the other hand, we further confirm that the forward Euler method gives less consistent results as the sampling frequency decreases, with either load torque model.

TABLE V
MOTOR M1 - IDENTIFIED PARAMETERS: COMPARISON BETWEEN DIFFERENT LOAD MODELS. WE HIGHLIGHT IN BOLD THE PARAMETERS THAT ARE SIGNIFICANTLY DIFFERENT FROM THE OPTIMUM ONES.

	Input Preview			
	4.8 kHz with T_{l_0}	4.8 kHz without T_{l_0}	2.4 kHz with T_{l_0}	2.4 kHz without T_{l_0}
R_s	0.48	0.48	0.48	0.48
R_r	0.21	0.21	0.21	0.21
X_l	0.30	0.30	0.30	0.30
X_m	11.29	11.29	11.28	11.28
J_r	0.26	0.26	0.26	0.26
T_{l_0}	0	-	0	-
T_{l_1}	0.037	0.037	0.037	0.037
	Euler			
	4.8 kHz with T_{l_0}	4.8 kHz without T_{l_0}	2.4 kHz with T_{l_0}	2.4 kHz without T_{l_0}
R_s	0.53	0.53	0.55	0.57
R_r	0.22	0.22	0.24	0.22
X_l	0.28	0.28	0.26	0.26
X_m	**2.52**	**2.52**	**1.45**	**1.36**
J_r	0.24	0.24	0.19	0.2
T_{l_0}	0	-	**13.21**	-
T_{l_1}	**0.13**	**0.13**	**0.20**	**0.24**

VI. CONCLUSION AND FUTURE DIRECTIONS

The presented experimental study shows that commercial circuit breakers can collect data with suitable quality to carry out an accurate parameter estimation of an induction machine. Algorithmic aspects have been discussed, and different variants of the identification algorithm have been compared, showing the superiority of the Input Preview discretization method over the forward Euler one. The approach can be used when stator measurements are available and the supplied voltage frequency is known, which makes its applicability difficult in presence of control devices such as a variable speed drive. This is subject of future research, as well as the use of the identified models to carry out motor detection and monitoring tasks, and to provide advanced protection by better discriminating between faults and motor inrush currents.

ACKNOWLEDGMENT

The authors would like to express their gratitude to Dr. Yannick Maret and Mr. Kevin Schaffner, for designing and assembling the sensor boxes, and to Dr. Mariusz Wojcik, Dr. Daniel Lewandowski, Dr. P. Lipnicki and Dr. M. Kaczmarek, for support during the electrical installation of the Emax2 and the AF38 contactors, and during the experimental tests.

REFERENCES

[1] X. Fang, S. Misra, G. Xue, and D. Yang, "Smart grid - the new and improved power grid: A survey," no. 14, pp. 944–980, 2012.
[2] ABB, "Load management with ekip power controller for sace emax 2," 2014.
[3] E. Ragaini, D. Angelosante, and L. Fagiano, "A method for identifying a fault event in an electric power distribution grid sector." Patent Application EP17 168 236, 2017.
[4] P. Waide and C. U. Brunner, "Energy-efficiency policy opportunities for electric motor-driven systems," 2011.
[5] Y. Koubaa, "Recursive identification of induction motor parameters," *Simulation Modelling Practice and Theory*, vol. 12, no. 5, pp. 363–381, 2004.
[6] F. Alonge, F. D'Ippolito, G. Ferrante, and F. Raimondi, "Parameter identification of induction motor model using genetic algorithms," *IEE Proceedings-Control Theory and Applications*, vol. 145, no. 6, pp. 587–593, 1998.
[7] T. Iwasaki and T. Kataoka, "Application of an extended kalman filter to parameter identification of an induction motor," in *Industry Applications Society Annual Meeting, 1989., Conference Record of the 1989 IEEE*. IEEE, 1989, pp. 248–253.
[8] M. Cirrincione, M. Pucci, G. Cirrincione, and G.-A. Capolino, "A new experimental application of least-squares techniques for the estimation of the induction motor parameters," *IEEE Transactions on Industry Applications*, vol. 39, no. 5, pp. 1247–1256, 2003.
[9] K. Wang, J. Chiasson, M. Bodson, and L. M. Tolbert, "A nonlinear least-squares approach for identification of the induction motor parameters," *IEEE Transactions on automatic Control*, vol. 50, no. 10, pp. 1622–1628, 2005.
[10] M. Cirrincione, M. Pucci, G. Cirrincione, and G.-A. Capolino, "Constrained minimization for parameter estimation of induction motors in saturated and unsaturated conditions," *IEEE Transactions on Industrial Electronics*, vol. 52, no. 5, pp. 1391–1402, 2005.
[11] A. Proco and A. Keyhani, "Induction motor parameter identification from operating data for electric drive applications," in *Digital Avionics Systems Conference, 1999. Proceedings. 18th*, vol. 2. IEEE, 1999, pp. 8–C.
[12] S. R. Shaw and S. B. Leeb, "Identification of induction motor parameters from transient stator current measurements," *IEEE Transactions on Industrial Electronics*, vol. 46, no. 1, pp. 139–149, 1999.
[13] M. Vélez-Reyes, W. L. Fung, and J. E. Ramos-Torres, "Developing robust algorithms for speed and parameter estimation in induction machines," in *Decision and Control, 2001. Proceedings of the 40th IEEE Conference on*, vol. 3. IEEE, 2001, pp. 2223–2228.
[14] D. Angelosante, L. Fagiano, F. Grasso, and E. Ragaini, "Motor parameters estimation from industrial electrical measurements," in *25th European Signal Processing Conference (EUSIPCO)*, 2017, pp. 1041–1045.
[15] L. Fagiano, M. Lauricella, D. Angelosante, and E. Ragaini, "Identification of induction motors with smart circuit breakers," *arXiv:1804.07817*, available at https://arxiv.org/abs/1804.07817v1, 2018.
[16] P. Krause, O. Wasynczuk, and S. D. Sudhoff, *Analysis of electric machinery and drive systems*. IEEE press, 2002.
[17] J. Nocedal and S. Wright, *Numerical Optimization*. Springer, 2006.